Strojniški vestnik - Journal of Mechanical Engineering 56(2010)4, 253-259
UDC 531.2:621.822
Paper received: 23.02.2010
Paper accepted: 30.04.2010

Static Behaviour of Air Plane Pads: Comparison Between Different Feeding Solutions

Guido Belforte - Federico Colombo - Terenziano Raparelli - Andrea Trivella - Vladimir Viktorov
Politecnico di Torino, Department of Mechanics, Italy

Air bearings are used among the others to support and guide coordinate measuring machines and instruments. There are different feeding solutions adopted to obtain the required stiffness and damping, often it is also important to minimize the air consumption.

The purpose of this paper is to evaluate the effects of supply orifice number on the static characteristics of plane pad circular air bearings. Two solutions are experimentally investigated, with six and three supply inherent orifices of same dimensions.

A test bench is used to obtain the static characteristics (load capacity and mass flow rate) of the pads. Then the static pressure distribution under the pads are experimentally determined in different directions.

A numerical model is developed to simulate the behaviour of the pads; a comparisons between experimental and numerical results is presented.

Keywords: gas thrust bearing, discharge coefficients, inherent orifices feeding system, circular pad

0 INTRODUCTION

Gas bearings are widely used for that applications in which it is necessary to reduce friction and obtain high positioning precision.

Since ‘60 years these components have been studied both experimentally and theoretically in order to deepen the knowledge of the phenomena that control their behaviour and develop new technical solutions. Different are the contributions to the development of the base theory on gas lubrication [1]. Concerning the gas thrust bearings in [2] and [3] the air flow under orifice compensated circular pads is analysed and in particular the pressure distribution near the supply orifices is considered. In [4] different feeding systems i.e. pocketed and annular orifices are analysed and their effects to the pad load carrying capacity, stiffness and flow rate are studied. In [5] different numerical methods to simulated the pressure distribution under the pads are discussed. In [6] a supersonic thrust bearing is studied and more recently in [7] is described an experimental activity carried on rectangular pads. With particular attention to the dynamic properties, in [8] are analysed the stiffness and the damping coefficients of circular air pads subjected to periodic forces and in [9] the pressure perturbation at the edge of the bearing pocket is analysed during air hammer.

The results of numerical simulations on air pads with different orifice and porous feeding systems are shown in [10]. In [11] is presented an experimental study on the determination of the discharge coefficients with feeding systems with inherent orifices and pocketed orifices.

The present paper presents a numerical and experimental work on the static behaviour of circular air pads with inherent orifices. Two pads are compared, one with six and the other with three supply orifices with the same diameter situated on the same circumference. The test bench used to measure the static properties of the pad is described. The characteristics of load capacity, stiffness and air consumption of the pads are shown, with also the pressure distributions along the radial and the circumferential directions. A numerical model based on finite difference method is used to simulate the pads. It uses experimentally identified discharge coefficients to calculate the air flow through the supply orifices. The comparison of numerical and experimental results is discussed.

1 GEOMETRY OF THE PADS

The pads, both of external diameter ϕ_e = 40 mm, are visible in Fig. 1. They are provided with a vented camera of diameter ϕ_i =10 mm concentric with the pad. The pads present N

*Corr. Authors' address: Politecnico di Torino, Department of Mechanics, Corso Duca degli Abruzzi 24, Torino, Italy, andrea.trivella@polito.it

supply holes (Pad *1*: $N = 6$, Pad *2*: $N = 3$) located on a circumference of radius $r_S = 12.5$ mm and equally spaced. The holes are drilled on brass cylindrical inserts having diameter $d_0 = 4$ mm.

The length of the holes is $l = 0.4$ mm and their diameter d. Their shape and dimensions were verified with a microscope. The measured values of d for each orifice are reported in Table 1. The obtained values are the mean values measured along two orthogonal directions. For each pad is also reported the mean diameter value considering all N orifices.

Table 1. *Geometric parameters*

Pad type	*N*	*Orifice position*	*Measured orifice diameter d [mm]*	*Mean diameter value [mm]*
1	*6*	*1*	*0.228*	*0.221*
		2	*0.230*	
		3	*0.212*	
		4	*0.219*	
		5	*0.218*	
		6	*0.217*	
2	*3*	*1*	*0.237*	*0.222*
		2	*0.211*	
		3	*0.219*	

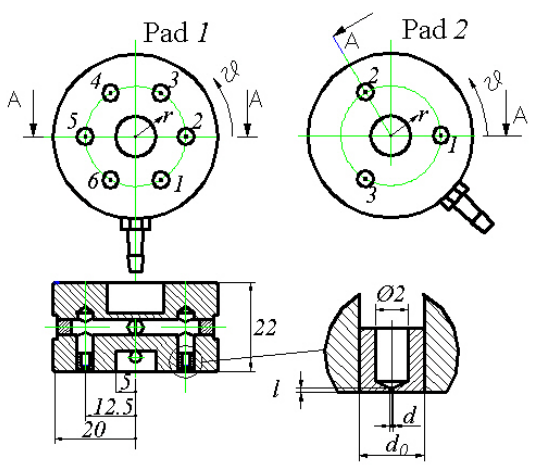

Fig. 1. *Sketch of the pads*

The superficial roughness of the pads was verified to be approximately $Ra = 0.4$ μm. In Fig. 2 are visible the pads and in Fig. 3 is shown the magnification of an orifice.

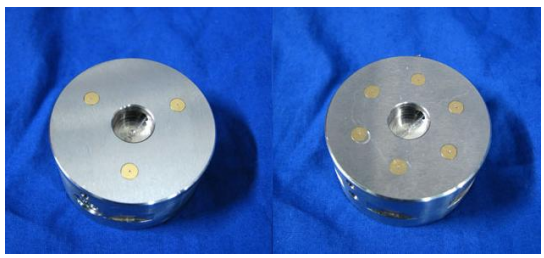

Fig. 2. *Photo of the pads*

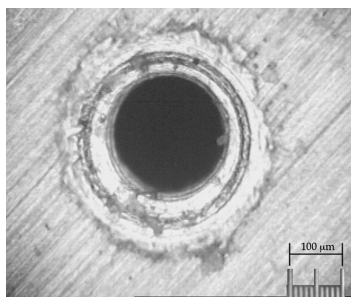

Fig. 3. *Enlargement of supply orifice 3, Pad 2*

2 MATHEMATICAL MODEL

The inlet mass flow rate G through a single supply port is given by ISO formula 6358 (1):

$$G = \begin{cases} C_S k_T P_S, & if \quad 0 < \dfrac{P_c}{P_S} < b \\ C_S k_T P_S \sqrt{1 - \left(\dfrac{\dfrac{P_c}{P_S} - b}{1 - b} \right)^2}, & if \quad \dfrac{P_c}{P_S} > b \end{cases} \tag{1}$$

where $C_S = 0.686 \dfrac{c_d S}{\sqrt{R^0 T^0}} \quad \left[\dfrac{\text{kg}}{\text{sPa}} \right]$ (2)

c_d is the discharge coefficient of the supply holes, P_s and P_c are the orifice upstream and downstream absolute pressures respectively. Isothermal expansion, compressible and laminar flow are assumed in the air gap. The Reynolds' equation (3) in polar coordinates is solved using the finite difference method:

$$\frac{1}{r}\frac{\partial}{\partial r}\left(rh^3 \frac{\partial P^2}{\partial r} \right) + \frac{1}{r^2}\frac{\partial}{\partial \vartheta}\left(h^3 \frac{\partial P^2}{\partial \vartheta} \right) + 24\mu R^0 T^0 q = 24\mu \frac{\partial (Ph)}{\partial t} \tag{3}$$

where $q = G/(r\, dr\, d\vartheta)$.

The discharge coefficient c_d is obtained using the empirical Eq. (4) and results as a function of h, d, and Re [11]:

$$c_d = 0.85\left(1 - e^{-8.2\frac{h}{d}}\right)\left(1 - e^{-0.001\mathrm{Re}}\right) \quad (4)$$

where $Re = 4G / \pi d_S \mu$.

Being Re dependent on G, the determination of c_d is iterative until convergence.

The range of ratio h/d in which the Eq. (4) is interpolated is 0.01÷0.1.

The considered boundary conditions are:

- $P = P_a$ at inner and outer radius;
- $P = P_c$ downstream the supply orifices.

The Reynolds equation was discretized with finite difference method with a grid of 20 nodes along the radial direction and 72 nodes along the circumferential direction between two adiacent orifices.

3 TEST BENCH AND TEST PROCEDURE DESCRIPTION

The static characteristics of the pad are experimentally determined with the test bench of Fig. 4.

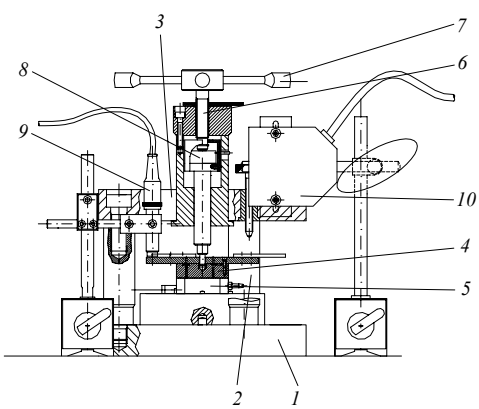

Fig. 4. *Sketch of the test bench*

The set-up frame consists of a base (1), three columns (2) and a crossmember (3). The air gap h is established between the pad under test (4) and stationary bearing member (5). Pad (4) can be moved vertically by means of screw (6) and handwheel (7). The force on the pad is monitored by an estensimetric load cell (8) with full range 2 kN. The air gap is monitored by three no contact inductive transducers (9) equispaced at 120°, with resolution 0.1 μm. A laser beam (10), visible also in Fig. 5, is used to calibrate *in loco* the gain of each inductive sensor. The air flow rate is measured by a flow meter situated upstream the pad.

A measuring hole of diameter 0.2 mm is provided in the stationary bearing member and connected to a piezoresistive pressure transducer that measures the pressure in the air gap with a precision of 10^{-4} MPa. In order to read the pressure in the air gap the stationary bearing member is translated radially by a screw or it is rotated. Its radial position is read by an LVDT. In this way the pressure in correspondence of the measuring hole can be measured along the radial or the circumferential direction.

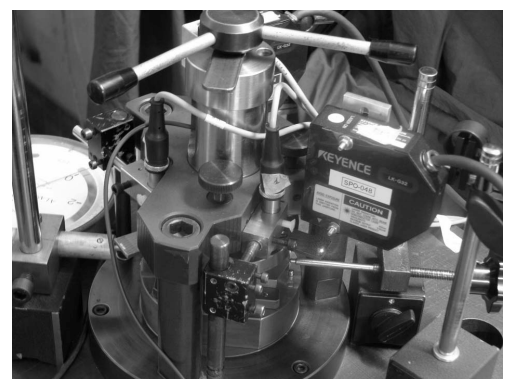

Fig. 5. *Photo of the test bench*

The pads characteristics are strongly influenced by the supply pressure value and the air clearance. An operating procedure was defined in order to obtain accurate and repeatable measures of the air clearance h. The pad, supplied with compressed air, is loaded by handwheel (7) with an increasing downwards vertical force until the air clearance is equal to zero. In this condition the displacement transducers are set to zero. In this way the reading of the displacement transducers coincides with the air clearance. Higher loads are avoided in order not to deform the pad and the stationary member.

During the determination of the static characteristic the air clearance, averaged among the three transducers readings, is increased in the range 3÷20 μm and the air flow and the force are measured.

All measures are relative to P_s = 0.6 MPa. Once the air clearance is imposed, the supply pressure is corrected in order to keep it constant.

The pressure distributions under the pad were measured with detail near the supply orifices because the pressure gradients are high.

4 EXPERIMENTAL RESULTS

The static characteristics of the pads are shown in Figs. 6 to 8. Pad *1* reaches a higher load carrying capacity and expends more air flow than Pad *2*. There is a maximum load capacity for low clearances, at about $h = 6$ μm. As shown in Fig. 7 for both pads the highest stiffness is obtained approx. at $h = 13$ μm. The optimum bearing clearance for static stiffness reduces with increasing the number of supply orifices *N*.

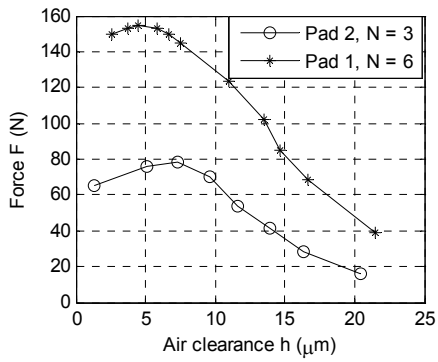

Fig. 6. *Load capacity F of Pad 1 and Pad 2, P_s=0.6 MPa*

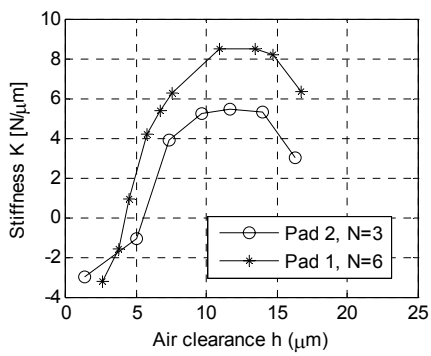

Fig. 7. *Stiffness K of Pad 1 and Pad 2, P_s=0.6 MPa*

The pressure distributions under the pads were measured with $h = 15$ μm. The radial distributions shown in Fig. 9 are relative to the plane in correspondence of the supply orifice ($\vartheta = 0°$) and to the middle plane between two supply orifices ($\vartheta = 60°$ for Pad *1* and $\vartheta = 30°$ for Pad *2*). The radial pressure distributions are not symmetric with respect to the position of coordinate r_S; this is more evident for radial planes far away the two supply orifices. This effect is due to the lower resistance of the air clearance towards the outside than towards the inside of the pad.

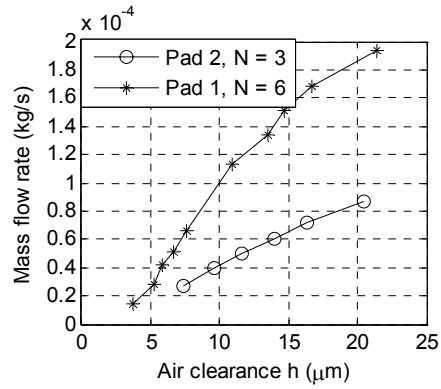

Fig. 8. *Air mass flow rates of Pad 1 and Pad 2, P_s=0.6 MPa*

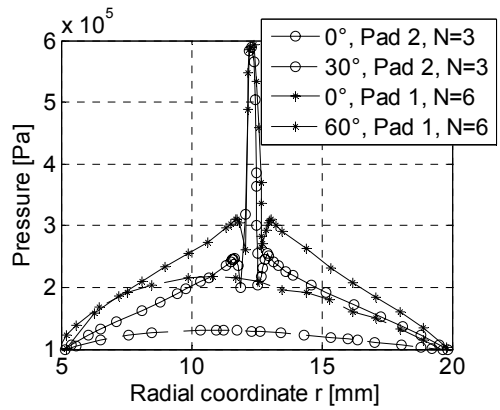

Fig. 9. *Radial pressure distributions in correspondence of orifice 3 (Pad 2) and orifice 4 (Pad 1), h=15 μm, P_s=0.6 MPa*

The circumferential pressure distribution is measured along the supply circumference of radius r_S between two supply orifices, see Fig. 10. For Pad *2* the circumferential pressure distribution decreases approximately to ambient pressure. In this case the holes can be considered almost independent and the pad surface is not well used. It is evident that both radial and circumferential pressure distributions increase with the number of supply orifices *N*.

The experimental pressure distributions change strongly in correspondence of the supply orifices due to the flow inertial effects. For example Fig. 11 shows a detail of the radial pressure distribution.

The maximum pressure measured under the supply orifice is almost equal to the supply pressure P_s. Increasing the distance from the centre hole the pressure decreases first strongly and then increases until a local maximum. It was verified [11] that with hole diameter between 0.2 to 0.4 mm and air gap h between 10 to 20 μm the local maximum of pressure is positioned with sufficient approximation at a distance $40 \cdot h$. The discharge coefficient c_d given from the empirical Eq. (4) allows to obtain a numerical pressure P_c close to the experimental local maximum. Beyond the local maximum the pressure decreases more gradually due to viscous actions and the pressure distribution can be calculated with Eq. (3).

The local maxima along the radial and the circumferential direction coincide. For this reason the empirical experimental discharge coefficient can be calculated considering both the radial and the circumferential pressure distributions.

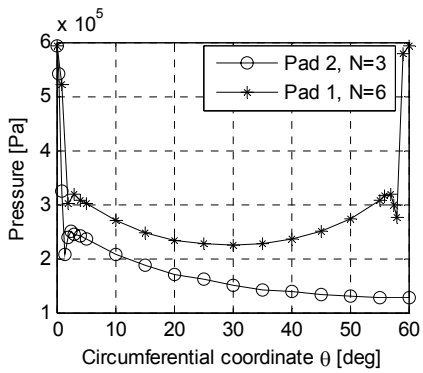

Fig. 10. *Circumferential pressure distributions between orifices 3 and 1 (Pad 2) and between orifices 4 and 5 (Pad 1), h=15 μm, P_s=0.6 MPa*

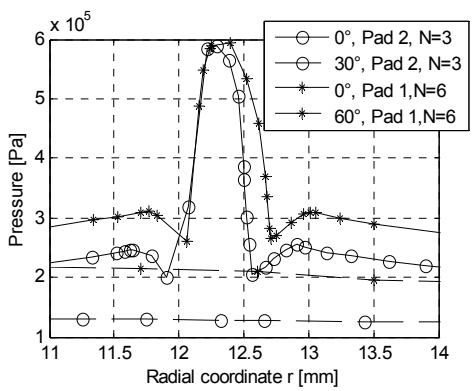

Fig. 11. *Detail of Fig. 9*

5 COMPARISON BETWEEN NUMERICAL AND EXPERIMENTAL RESULTS

The experimental data are compared with numerical results obtained integrating Reynolds equation. In Figs. 12 to 15 the experimental and the numerical radial pressure distributions with h = 15 μm and P_S = 0.6 MPa are compared. Figs. 12 and 13 are relative to the radial and circumferential pressure distributions under Pad *1* and Figs. 14 and 15 under Pad *2*. The comparison of the results is valid for distances from the supply holes greater than 40 h because the model does not take into account pressure and velocity gradients under the supply holes. The numerical value of P_c can be compared with the experimental local maximum of pressure.

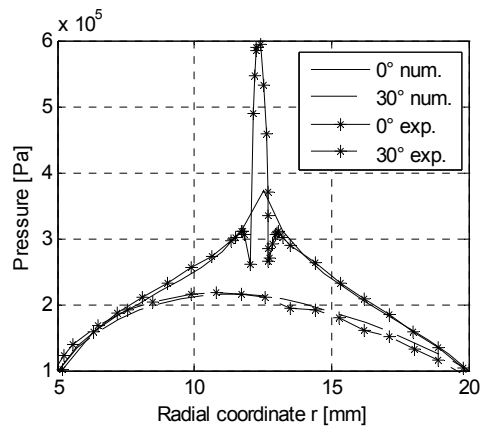

Fig. 12. *Comparison of experimental and numerical radial pressure distributions, Pad 1, h=15 μm, P_S =0.6 MPa*

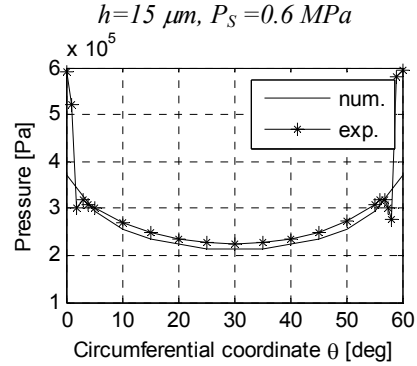

Fig. 13. *Comparison of experimental and numerical circumferential pressure distributions, Pad 1, h=15 μm, P_S =0.6 MPa*

For Pad *1* the numerical and experimental pressure distributions are quite in good

accordance in the zone of laminar flow. In correspondence of the hole the numerical downstream pressure P_c is about 20% higher than the experimental local maximum. For Pad *2* the difference between numerical and experimental values can be due to the tolerance error in measuring the air clearance under the pad. The pressure distribution, in fact, is very sensitive to this parameter.

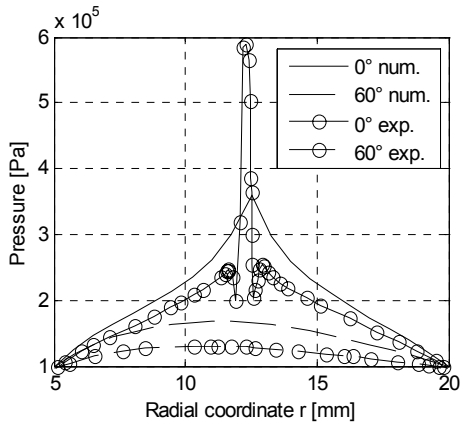

Fig. 14. *Comparison of experimental and numerical radial pressure distributions, Pad 2, h=15 μm, P_S =0.6 MPa*

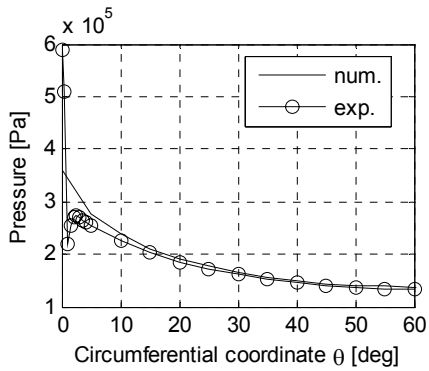

Fig. 15. *Comparison of experimental and numerical circumferential pressure distributions, Pad 2, h=15 μm,P_S =0.6 MPa*

6 CONCLUSIONS

The following conclusions can be stated:

- the load carrying capacity and the air mass flow rate with six orifices are approximately twice than that obtained with three orifices, but at higher clearances it is convenient to use a lower number of supply orifices because the air flow increase predominates;
- the load capacity of the pad with six supply orifices suffers less of the effect of negative stiffness at low clearance because the pressure distribution is more uniform in the pad surface;
- the optimum bearing clearance for static stiffness reduces with increasing the number of supply orifices;
- numerical and experimental results are quite in good agreement, considering the tolerance in the experimental measure of the air clearance and the high sensitivity of flow rate and pressure to a clearance variation. The model can be used to simulate and optimize the geometry of pads with several orifices.

6 ACKNOWLEDGEMENTS

This work was supported by MIUR: PRIN project: "Study and development of gas bearings for ultra high speed electrospindle", 2006; FIRB project "Enabling technologies for multitasking high precision machining of microparts", 2007.

7 NOMENCLATURE

b	Critical pressure ratio
c_d	Discharge coefficient of supply orifices
d	Supply orifice diameter
d_0	Insert diameter
k_T	Temperature coefficient = $\sqrt{T^0 / T}$
l	Supply orifice length
h	Air clearance
q	Inlet mass flow rate per unit area
r	Radial coordinate
r_S	Radius of supply circumference
N	Number of supply orifices
P	Absolute pressure
P_a	Absolute ambient pressure
P_s	Absolute supply pressure
P_c	Absolute supply orifice downstream pressure
R^0	Gas constant = 287.6 m^2/s^2K
T^0	Absolute temperature in normal condition = 293 K
T	Absolute orifice upstream temperature
Re	Reynolds number
S	Supply orifice cross section
ϑ	Circumferential coordinate

ϕ_e Pad external diameter
ϕ_i Pad internal diameter
μ Air viscosity = 17.89 10^{-6} Pa s

8 REFERENCES

[1] Gross, W.A. (1962) Gas film lubrication, Wiley, New York.

[2] Mori, H., Miyamatsu, Y. (1969). Theoretical flow-models for externally pressurized gas bearings, *Journal of Lubrication Technology*, vo. 91, no. 1 p.181-193.

[3] Poupard, H., Drouin, G. (1973) Theoretical and experimental pressure distribution in supersonic domain for an inherently compensated circular thrust bearing. *Journal of Lubrication Technology*, vol. 95, no. 3, p. 217-221.

[4] Kazimierski, Z., Trojnarski, J. (1980). Investigations of externally pressurized gas bearings with different feeding systems. *Journal of Lubrication Technology*, vol. 102, no. 1, p. 59-64.

[5] Al-Bender, F. van Brussel, H. (1992) Symmetric radial laminar channel flow with particolar reference to aerostatic bearings. *Journal of Tribology*, vol 114, p. 630-635.

[6] Miyake,Y., Inaba, T., Kubo, N., Takeoka, J. 1985) An experimental study on externally pressurized supersonic gas thrust bearings. *Journal of Tribology*, vol. 107, no. 1, p. 122-127.

[7] Kassab, S.Z., Noureldeen, E.M., Shawky, M.A. (1997) Effects of operating conditions and supply hole diameter on the performance of a rectangular aerostatic bearing. *Tribology International*, vol 30, no. 7, p. 533-545.

[8] Stiffler, A.K. (1974) Analysis of the stiffness and damping of an inherently compensated, multiple-inlet, circular thrust bearing, *Journal of Lubrication Technology*, p. 329-336.

[9] Boffey, D.A., Wilson, P.M. (1981) An experimental investigation of the pressure at the edge of a gas bearing pocket. *Journal of Lubrication Technology*, vol. 103, no. 10, p. 593-600.

[10] Fourka, M., Bonis, M. (1997) Comparison between externally pressurized gas thrust bearings with different orifice and porous feeding systems. *Wear*, vol. 210, p. 311-317.

[11] Belforte, G., Raparelli, T., Viktorov, V., Trivella, A. (2007) Discharge coefficients of orifice-type restrictor for aerostatic bearings, *Tribology International*, vol. 40, p. 512-521.